



Investigation of the cell structure and organelles during autolytic PCD of *Antirrhinum majus* “Legend White” petals

Roghayeh Nabipour Sanjbod¹ · Esmaeil Chamani¹ · Younes Pourbeyrami Hir¹ · Asghar Estaji¹

Received: 17 March 2022 / Accepted: 18 June 2022

© The Author(s), under exclusive licence to Springer-Verlag GmbH Austria, part of Springer Nature 2022

Abstract

One of the classes of the plant developmental programmed cell death (PCD) is vacuolar cell death or autolysis. The results of the transmission electron microscope (TEM) studies indicated that this type of PCD occurs during the petal senescence of *Antirrhinum majus* “Legend White” flowers. The major hallmarks of the process related to the ultrastructure of the cells involved chloroplast degradation, vacuolation, chromatin condensation, cell wall swelling, degradation of Golgi apparatus, protoplasmic shrinkage, degradation of the endoplasmic reticulum, nuclear fragmentation, rupture of tonoplast, and plasma membrane. Macroautophagy and microautophagy processes were also clearly observed during vacuole formation. As in yeasts, in the present study, Golgi apparatus became autophagosome-like structures during degradation that had autophagy activity and then disappeared. Our results revealed a type of selective microautophagy, piecemeal microautophagy of the nucleus (PMN), in nuclear degradation during PCD of petals that has not previously been reported in plants. Moreover, vesicular structures, such as paramural and multilamellar bodies, were observed in some stages.

Keywords *Antirrhinum majus* “Legend White” · Autophagy · Organelles structure · Programmed cell death · Petal senescence · TEM analysis · Ultrastructural changes

Introduction

Petal senescence, a genetically programmed and irreversible event, is often considered synonymous with programmed cell death (PCD) and closely related to pollination and is not affected to a large extent by environmental stresses (Wagstaff et al. 2003; Azad et al. 2008; Van Doorn and Woltering 2008; Rogers 2015; Ma et al. 2018). PCD involves numerous physiological processes, from germination to senescence of

whole organs (Wagstaff et al. 2003). Van Doorn (2011) has classified PCD into two main classes based on morphological criteria: vacuolar cell death (or autolysis) and necrotic cell death (or necrosis). Vacuolar cell death or autolytic PCD mainly occurs during the normal development of plants and abiotic stresses (Van Doorn et al. 2011; Van Doorn 2015). The critical characteristics of the vacuolar cell death include: the cytoplasmic volume decrease accompanying an increase in lytic vacuoles volume, autophagy-like processes, tonoplast rupture, and destruction of cytoplasmic components. Necrotic cell death is distinguished from vacuolar cell death by features including mitochondrial swelling, absence of lytic vacuoles, early rupture of the plasma membrane, protoplast shrinkage, and unprocessed cell corpse. Necrosis is considered non-autolytic PCD and is typically triggered by a pathogen attack (Van Doorn 2011, 2015; Van Doorn et al. 2011; Shibuya et al. 2016).

After the beginning and progression of senescence, considerable changes occur at the morphological, physiological, cellular, and molecular levels (Zhao et al. 2018). Cellular structural changes associated with senescence have typically occurred before the visible symptoms of PCD of petals or even before fully opened flowers (Van Doorn et al. 2003;

Handling Editor: Peter Nick

✉ Esmaeil Chamani
echamani@uma.ac.ir
Roghayeh Nabipour Sanjbod
rnabipour@uma.ac.ir
Younes Pourbeyrami Hir
younes_ph62@uma.ac.ir
Asghar Estaji
aestaji@yahoo.com

¹ Department of Horticultural Sciences, Faculty of Agriculture and Natural Resources, University of Mohaghegh Ardabili, Ardabil, Iran

Wagstaff et al. 2003; Breeze et al. 2004). Cell walls, a rigid preclude to phagocytosis and plant cell swelling, are targeted by PCD changes such as plant cell wall swelling and gradual disappearance (O'Donoghue 2006; Van Doorn et al. 2011; Shibuya et al. 2016). Some researchers have confirmed this in species such as *Dendrobium*, *Iris* (Kamdee et al. 2015), and *Sandersonia* (O'Donoghue et al. 2002). In necrosis, the irreversible detachment of the plasma membrane from the cell wall or protoplast shrinkage is one of the morphological hallmarks of cell death (Van Doorn et al. 2011; Minina et al. 2021). Studies have indicated that the nuclear morphology varies depending on the species (Van Doorn and Woltering 2008). During petals senescence in carnation, the nuclei were smaller and horseshoe-shaped (Smith et al. 1992). The chromatin condensation and nuclear fragmentation were observed in *Petunia hybrida* and *Argyranthemum frutescens*. In *Antirrhinum majus*, chromatin fragmentation occurred without nucleus fragmentation (Yamada et al. 2006). During vacuolar (autolytic) cell death, the vacuole act as a lytic compartment and has autophagy-like activity (Van Doorn et al. 2011). The result of autophagy activity is tonoplast rupture and release of hydrolase enzymes (Van Doorn 2015). Tonoplast rupture ultimately causes extensive degradation of the cytoplasm and cell organelles in the senescing corolla of Morning Glory, cytoplasm shrinkage, and reduction in the size of the organelles in *Iris* and carnation (Winkenbach 1971; Smith et al. 1992). Other organelles' deaths are less known (Van Doorn and Woltering 2008). In *Dianthus caryophyllus*, the endoplasmic reticulum and ribosomes disappeared during senescence. The number of Golgi apparatus has also gradually decreased (Smith et al. 1992). Some plastids and mitochondria also survived to the late stage of senescence. As the organelles disappeared, the volume of the cytoplasm also reduced (Winkenbach 1971).

The principal mechanism of vacuolar (autolytic) cell death is the gradual decrease of cytoplasmic content by lytic vacuoles, which is similar to autophagy-like processes in animals and yeasts (Van Doorn et al. 2011; Shibuya et al. 2016; Mondal et al. 2021). Researchers have suggested that three types of autophagy occur in plant systems. The macroautophagy process is performed by autophagosome-like organelles containing hydrolases (Van Doorn and Papini 2013; Sieńko et al. 2020). Macroautophagy has been reported extensively in cell death studies, such as *Lobivia rauschii* (Papini et al. 1999), *Digitalis purpurea* (Gaffal et al. 2007), and *Arabidopsis* (Avci et al. 2008). Microautophagy is the direct uptake of cytoplasmic contents by tonoplast deformation (Sieńko et al. 2020). Microautophagy information has been obtained based on yeast species. There is less evidence to prove it in plants, and it has been observed in limited cases (Van Doorn 2015), such as transport of cytoplasmic anthocyanin aggregates (Chanoca et al. 2015), chlorophagy (Nakamura et al. 2018), sucrose starvation (Goto-Yamada

et al. 2019), and vacuole development. Mega-autophagy is involved at the end of PCD and causes complete cell degradation after tonoplast rupture (Wertman et al. 2012; Van Doorn et al. 2015).

Despite extensive studies on various aspects of vacuolar (autolytic) cell death, there is still insufficient information on the sequence of events involved in the progression of senescence and death and the process of organelles degradation, especially in the Golgi apparatus and the endoplasmic reticulum. The hypothesis that has been put forward is that autophagy processes have a potential role in advancing the vacuolar (autolytic) cell death process. However, the available reports have been obtained based on yeasts as a model for plant studies, and there is still insufficient evidence to prove them, especially microautophagy, in plants. In addition, no suitable plant model has been proposed to study these processes in plants. Snapdragon (*Antirrhinum majus* L.) is a short-lived perennial plant that has been used as a model plant for genetic studies since the early twentieth century and recently is considered a model system with appropriate characterization for the study of flower development. However, its cell death has been less studied (Muhlemann et al. 2012; Rabiza-Świder et al. 2020). Therefore, our aim in this study was to investigate the possibility of autophagy processes and a comprehensive understanding of structural changes and morphology of organelles during vacuolar (autolytic) cell death. Hence, we used the TEM method to provide visual evidence and examined the mesophyll cells of the petals of the *Antirrhinum majus* "Legend White" flower from the flower bud stage to the last stage of senescence.

Materials and methods

Plant materials and growth conditions

Snapdragon F1 (*Antirrhinum majus* "Legend White") seeds were obtained from Takii Seed Company and germinated in Petri dishes at 20 °C under white LED light with a light intensity of 3000 lx. Coeval germinated seeds were selected and sown in plastic pots (length = 18 cm and height = 15 cm) containing a mixture of soil used for flower cultivation. The ratio of vermicompost to complete organic fertilizers in the soil mixture was 3:1. Pots were transferred to the greenhouse in December and grown under the temperature from 15 to 18 °C and in natural daylight. The plants were irrigated once every 2 days. Before flowering, the plants were transferred to a growth chamber with 20 °C temperature, 60% RH, and a 16/8 h day/night cycle. As described in Table 1, flower longevity was divided into several stages to investigate petal development and senescence. The sampling stage began from the flower bud stage, 9 days before flower opening, to

Table 1 Definition of floral stages during development and senescence of *Antirrhinum majus* “Legend White”

Stage	Relative day to the flower opening	Description of the floral features
S1	−9	Tight green bud
S2	−6	Emerging bud
S3	−3	Full bud
S4	0	Half-opened flower
S5	+3	Fully opened flower
S6	+6	Flower starting to wilt
S7	+9	Collapsed flower
S8	+12	Desiccated flower

12 days after flower opening. The first florets were analyzed to study 8 stages of petal cell development and death.

TEM

For transmission electron microscopy (TEM), we used the first florets at each stage. At the flower bud stages (S1, S2, and S3), the sepals were gently separated with a scalpel blade and the petals warily opened with a soft brush. The samplings of petal tissue pieces (approximately $2 \times 2 \text{ mm}^2$) were performed from the margin of the dorsal petal (upper lip) using a fresh sharp blade under a stereomicroscope (HUND WETZLAR, Helmut Hund, Germany). The samples were immediately fixed in 3% glutaraldehyde: 4% formaldehyde in 0.1 M phosphate buffer saline (PBS, pH 7.2) for 2 h at 4 °C. Then rinsed three times with the same buffer (10 min each time) and transferred to the TEM laboratory. Subsequent fixation was performed in 1% OsO₄ solution (in 0.1 M phosphate buffer) at room temperature for 2 h in a chemical fume hood. Afterward, the samples were washed three times with 0.1 M PBS (10 min each time). Fixed materials were then dehydrated using ascending graded series of alcohol, acetone, and acetone-resin mixture (50/50). Finally, the samples were embedded in epoxy resin (TAAB Embedding Resin, TAAB Laboratories Equipment Ltd, England) and polymerized at 60 °C for 48 h. Ultrathin cross-sections (50–100 nm) were obtained using an ultramicrotome (Leica Ultracut-R ultramicrotome, Wetzlar, Germany) and collected on standard 200 mesh copper grids. The positive stain was firstly performed in 20% uranyl acetate solution in pure methanol for 20 min. Then, the samples were stained with Reynolds solution (lead nitrate and sodium citrate) for 5 min (Reynolds 1963). TEM micrographs of mesophyll cells were acquired using a transmission electron microscope (EM208S, PHILIPS, Nederland) at operating 100 kV. Micrographs included the complete cell structure imaging and intracellular organelles with different magnification that were analyzed using ImageJ software version 1.52. All

micrographs were taken from mesophyll cells and none of the observations related to epidermal cells. In each micrograph, the wall thickness of one cell was analyzed, and ten micrographs were used per stage.

Statistical analysis of the data

Data were analyzed using SAS V9.2 software. Statistical analysis using one-way analysis of variance, at $P=0.95$. Means were compared using Duncan’s multiple range test at 1% and 5% probability levels, and data were given as the mean \pm SD. In this study, we drew a presented graph by GraphPad Prism8 software.

Results

Description of development and senescence stages of *Antirrhinum majus* “Legend White” flowers.

Antirrhinum majus “Legend White” has single flowers with five merged petals that form a corolla of flowers. In this study, each stage was named Stage 1: S1, Stage 2: S2..., and Stage 8: S8. At S1 (tight green bud), sepals have fully enclosed the flower and loosened. At S2 (emerging bud), the tips of the petals were visible. Stage 3 (full bud) was before the petal unfurls. At S4, the flower opened in half. At S5, the petals and anthers fully opened. As the flower senescence, the petals showed visible PCD-related wilting, so that at S6, despite the maximum expansion of petals, the first signs of wilting appeared at the margins of all the petals. At this stage, the color of the petals changed, and the translucence of the petal margins occurred. At S7, the wilting was severe, and after this stage, the petals completely desiccated within three days and remained attached to the plant (Fig. 1).

Cell arrangement

TEM analysis showed notable changes in cell arrangement across the petal mesophyll cells. At S1, the cells have an ovoid structure and arrange alongside regularly. There is some looseness in the arrangement of cells due to intercellular spaces (Fig. 2a). As the bud develops and the vacuole turgor pressure increases, the petals expand. At S4, the cells have maximum turgor pressure and regular organization (Fig. 2b). As the petals senescence, the cellular arrangement becomes disorganized, and the cells shrink so that, at S7, the mesophyll cells lose their organelles, the cellular contents disappear, and the cells compress (Fig. 2c).

Cell wall

TEM micrographs and the results of cell wall thickness revealed two decreases and one increase in cell wall

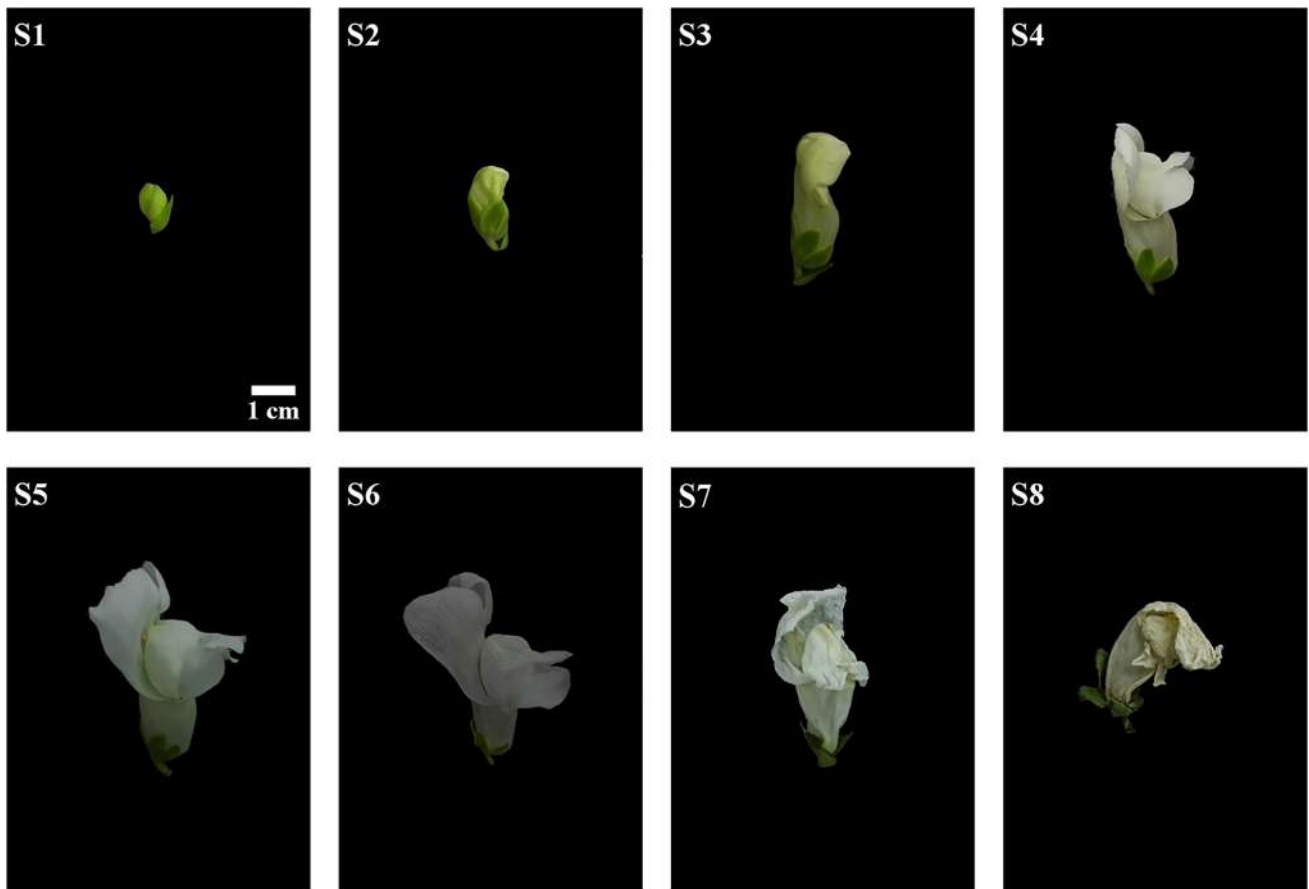
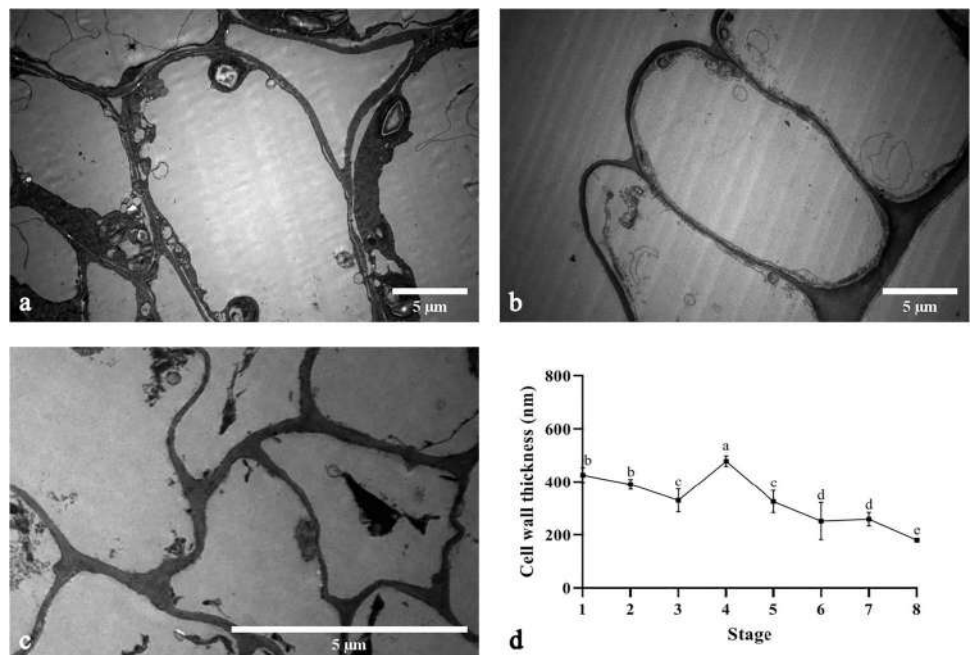


Fig. 1 Stages of development and senescence of *Antirrhinum majus* “Legend White” flowers and time to petal wilting and desiccation. S1: tight green bud; S2: emerging bud; S3: full bud; S4: half-open

flower; S5: fully open flower; S6: flower is starting to wilt; S7: flower collapsed; S8: flower desiccated. The scale is the same in all pictures

Fig. 2 Cell arrangement and cell wall thickness changes during stages of development and senescence of petal mesophyll cells of *Antirrhinum majus* “Legend White.” **a** Ovoid and regular cell structure with large intercellular spaces at S1; **b** regular cell organization with a large central vacuole at S4; **c** disorganization of mesophyll cells at S7; **d** cell wall thickness changes in different stages



thickness. A slight reduction in cell wall thickness was related to the stages before flower opening (S1 to S3). With reaching S4, there was an increase in cell wall thickness. Subsequently, after S4, the cell wall thickness decreased as the flower senescence, reaching a minimum size at S8, indicating degradation of the cell wall during vacuolar (autolytic) cell death (Fig. 2d).

Plasma membrane

At all stages of bud development (S1, S2, and S3) and S4, the plasma membrane had an entirely uniform structure and was located adjacent to the cell wall. At S5, the plasma membrane detached from the cell wall in many areas (Fig. 3a, arrows). This detachment continued until S6 so that the plasma membrane and the cytoplasm were concentrated in the central part of the cell (Fig. 3b, arrows). During S7, rupture of the plasma membrane was observed in some areas (Fig. 3c, arrow). As the petals desiccated, the plasma membrane disappeared entirely.

Nucleus

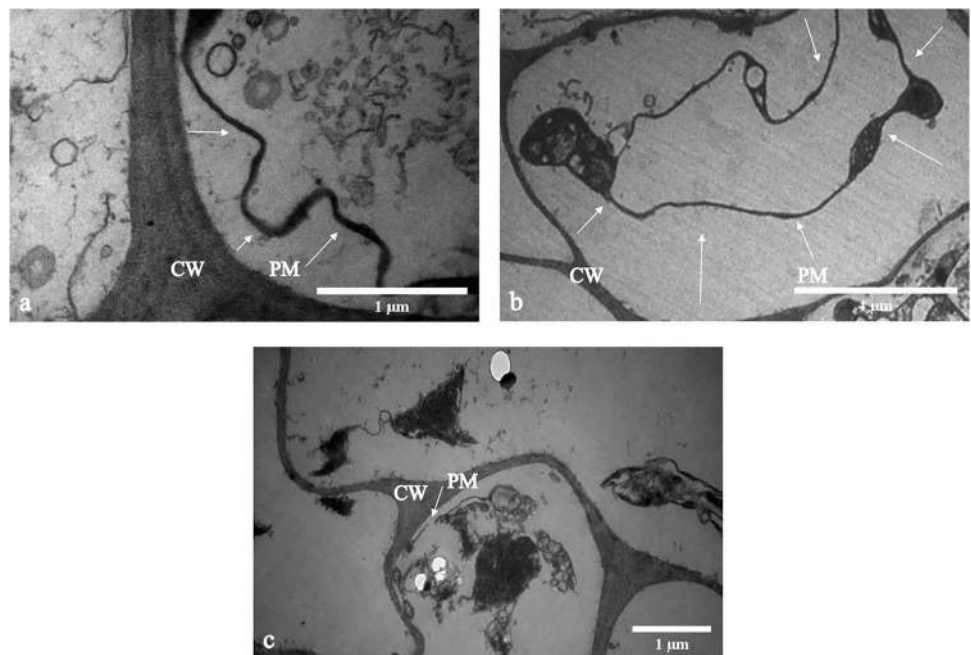
At S1 and S2, mesophyll cells had ovoid-shaped nuclei and natural size. Several compact nucleoli of different sizes were observed at these stages, and the chromatin condensation was homogeneous at the nucleus surface (Fig. 4a and b). At S3, the cells had an elongated nucleus with fewer nucleoli. As well as, some areas of the nucleus periphery showed partial chromatin condensation (Fig. 4c). At S4, the chromatin condensation was continued (arrows). The nuclei containing

nucleolus had an irregular shape, indicating that the chromatin was disintegrating and condensing (Fig. 4d). At S5, nuclear fragmentation was observed, and a fragment entered the vacuole (Fig. 4e, arrowhead). In addition, an interesting structure was observed. In a part of the nucleus, the bilayer membrane of the nucleus was protruding into a small vacuole. It formed a bleb that this event is similar to piecemeal microautophagy of the nucleus (Fig. 4e, small arrow). The nucleolus and clear chromatin condensation were still present (Fig. 4e, large arrows). At S6, the nucleus fragments were observed (Fig. 4f, arrows), the nucleus size was significantly reduced, and the nucleus was round and regular. Chromatin condensed throughout the nucleus's surface. The nucleus was attached to a small vacuole where chromatin appears shrunk on the nucleus's side (arrow). The nucleolus was destroyed. The nucleus membrane remained intact at all stages (Fig. 4f and g). At S7 and S8, no nucleus was observed in the cells, indicating the collapse of the nucleus at these stages.

Vacuole

At S1, the cells showed the early stages of vacuolation (Fig. 5a, arrows). They often had a dense cytoplasm and lots of spherical and small tubular fragments with a lower electron density than the cytoplasm with or without membrane. Arrows point to the tubes, which are aligned and form a new network in which tubes and spherical components are found. Also, a space similar to a vacuole has been created. At S2, tube structures with low electron density may fuse laterally to form a continuous space in the cytoplasm (large arrows).

Fig. 3 Plasma membrane ultrastructural changes during stages of development and senescence of petal mesophyll cells of *Antirrhinum majus* "Legend White." **a** Plasma membrane detachment at S5; **b** shrinking of the plasma membrane and cytoplasm in the central part of the cell at S6; **c** plasma membrane rupture at S7. CW cell wall, PM plasma membrane



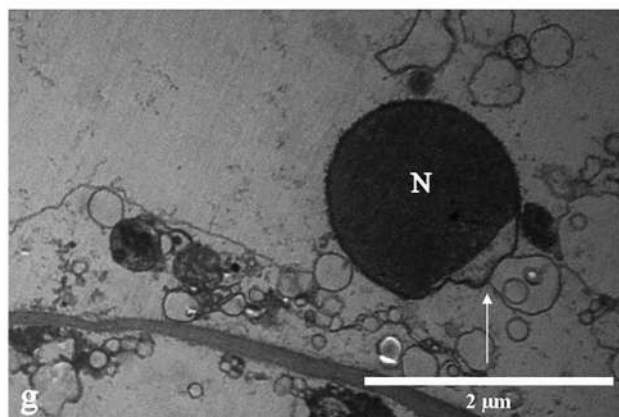
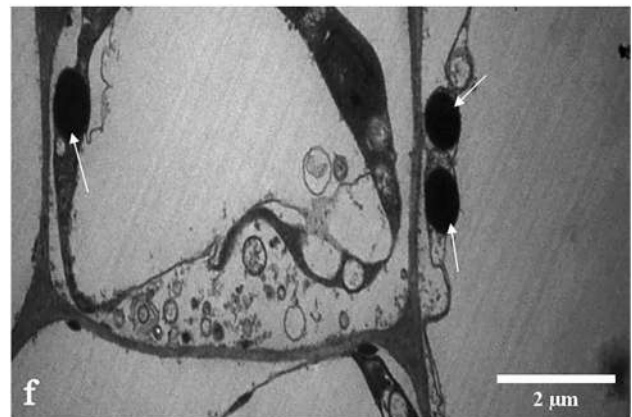
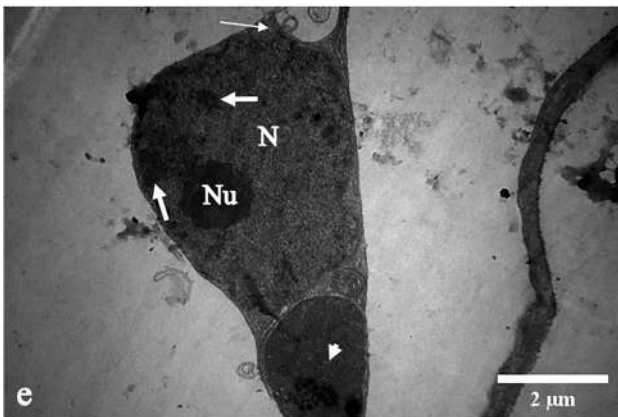
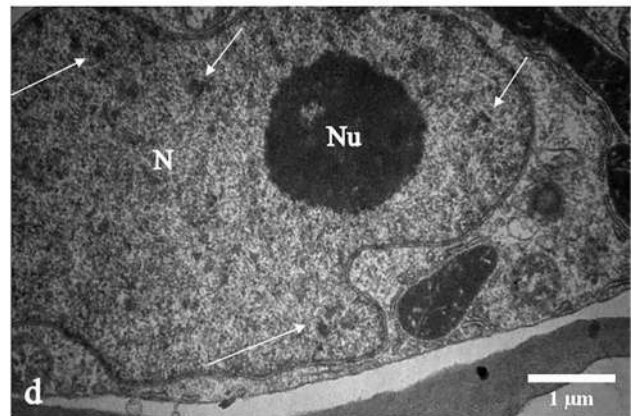
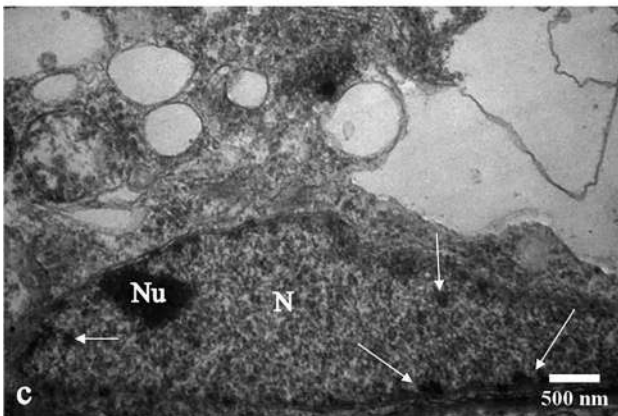
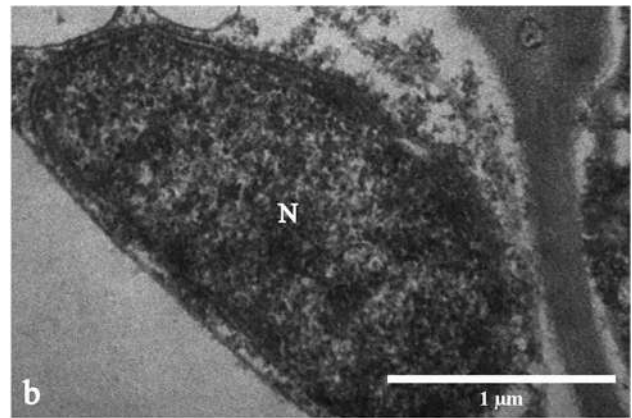
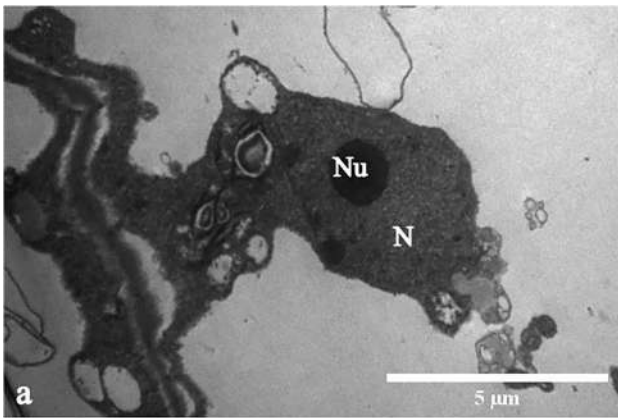


Fig. 4 Nucleus ultrastructural changes during stages of development and senescence of petal mesophyll cells of *Antirrhinum majus* "Legend White." **a** Normal morphology of nucleus at S1 and **b** S2; **c** partial chromatin condensation at S3; **d** the irregular shape of the nucleus at S4; **e** protruding of bilayer membrane of the nucleus into a small vacuole (piecemeal microautophagy of the nucleus (PMN)) at S5; **f, g** the nucleus fragments and significant reduction of nucleus size at S6. N nucleus, Nu nucleolus

There are many small vacuoles (small arrows) that may fuse. Also, the vacuoles have an actual membrane and are more extensive in size. These observations provide evidence for the onset of the macroautophagy in vacuolation (Fig. 5b, arrows). At Fig. 5c, the vacuole membrane protrudes in two parts. It seems a part of the cytoplasm is inside the vacuole. In one of these parts, even a membrane is formed. At the top of the micrograph, a smaller vacuole has a spiral structure with a high electron density attached to the cytoplasm (arrows). This process is common in microautophagy (Fig. 5c). At S3, an increase in central vacuole volume and a decrease in small vacuoles occurred due to the joining of small vacuoles to the central vacuole or the fusion of the vacuoles (Fig. 5d, arrows). When the flowers had just opened (S4), the cells had a large single vacuole with a uniform lumen and low electron density. Due to turgor pressure, a thin layer of cytoplasm and organelles was located adjacent to the cell wall (Fig. 5e). At S5, the central vacuole occupied the entire cell, but in some areas, the plasma membrane is detaching from the cell wall (Fig. 5f, arrows). At S6, tonoplast rupture occurred (arrow). The plasma membrane was intact and separated from the cell wall. Vacuole-like vesicles containing debris and membrane structures are attached to the central vacuole (Fig. 5g) inside the cytoplasm. At S7, the central vacuole was destroyed. Some protoplast remnants were seen in the cell, which was degraded by several small vacuoles (Fig. 5h).

Mitochondria

At S1, there were many round mitochondria with a natural ultrastructure and unrecognizable crista (Fig. 6a). At S2, two inner and outer membranes of mitochondrial and crista were detectable (Fig. 6b). At S3, the shape of mitochondria changed from round to elliptical in some cases. The cells at S4, S5, and S6 contained many elongated mitochondria with a dense matrix. There were dense electron granules of various sizes on the interior surface of the mitochondria (Fig. 6c and d). At S7, spherical sections with low electron density were observed at the mitochondria's surface, indicating degeneration in the crista structures (Fig. 6e, arrows). In most mesophyll cells at S8, either no mitochondria were present or, in a few cases, they appeared to be smaller in size (Fig. 6f).

Golgi apparatus

At S1, abundant Golgi apparatus was in the cell with 4–8 straight or curved cisternae, a distinct cis–trans polarity, and numerous vesicles, indicating their activity (Fig. 7a). At S2, the Golgi apparatus was actively in the cytoplasm (Fig. 7b). At S3, the number of Golgi apparatus and vesicles was lower, but they were still functionally active, and the cis–trans polarity was detectable in them (Fig. 7c). At S4, the Golgi apparatus had irregular organization, fewer cisternae, unclear cis–trans polarity, and no vesicles. In some cases, the cisternae curved and joined together to form an autophagosome-like structure that appeared to be a Golgi body in degradation. These structures had two membranes and cytoplasmic contents (Fig. 7d). No Golgi apparatus was observed later, indicating their early degradation after S4.

Endoplasmic reticulum

Mesophyll cells from S1 to S4 had a plentiful endoplasmic reticulum. They had independent cisternae scattered throughout the cytoplasm and organelles (Fig. 8a). At S5, the endoplasmic reticulum was partially observed in some parts of the cytoplasm (Fig. 8b) and disappeared at later senescence and cell death stages.

Chloroplast

Chloroplast at S1 had normal morphology, intact envelope membrane, recognizable granum, normal thylakoids, and large starch granules (Fig. 9a). At S2, degradation of chloroplasts was observed. The chloroplast envelope membrane was ruptured in sections, and the inner membrane systems (thylakoids and granum) lost their structure (Fig. 9b). Chloroplasts at the S3 had fewer granum, and dense electron globules were found on the surface of the chloroplast and between the grana. Starch granules were disappearing. The chloroplast envelope membrane was removed entirely (Fig. 9c). Finally, the chloroplasts disappeared and were not found in any mesophyll cells at S4.

PB

The results revealed paramural body (PB) formation between the cell wall and the plasma membrane. At S1, two vesicles with membranes and different sizes were observed (Fig. 10a). At S2, two vesicles were observed that formed from the plasma membrane (Fig. 10b). Mesophyll cells have vesicles of various shapes with or without an outer membrane at S3 (Fig. 10c). At S4, the vesicles have other vesicles inside (Fig. 10d). PB at S5 had different shapes, such as

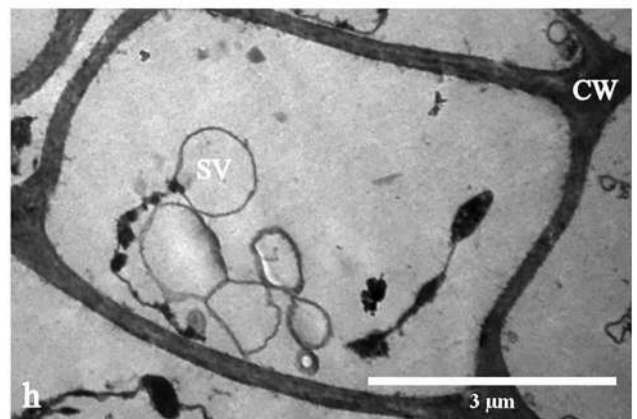
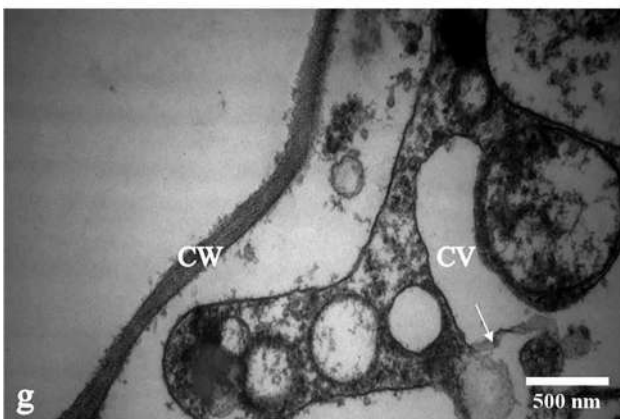
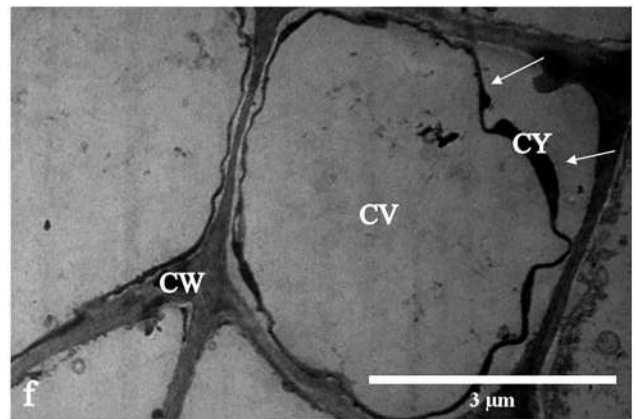
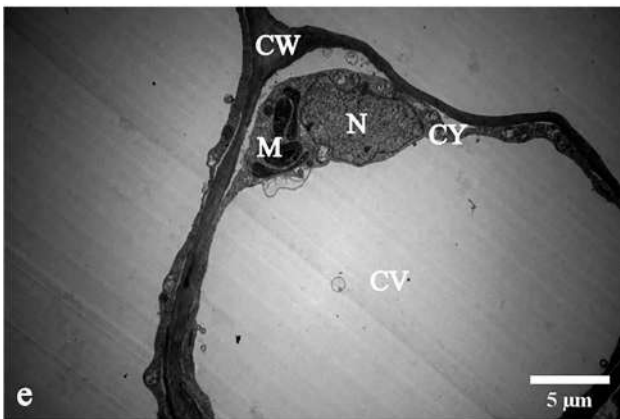
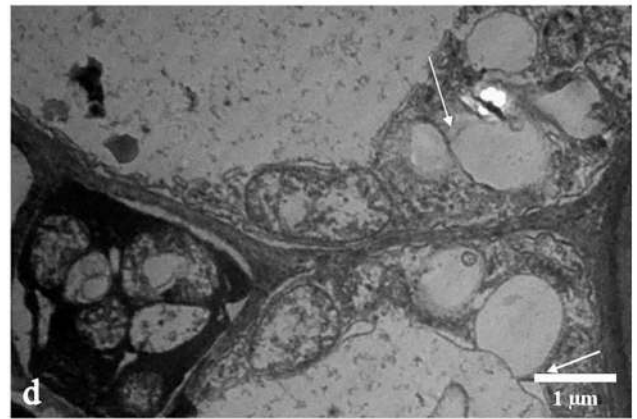
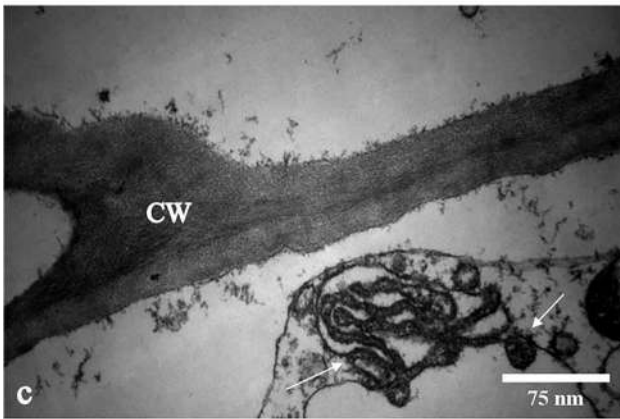
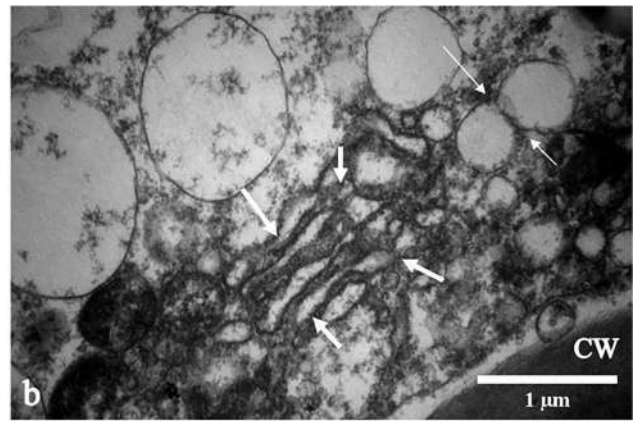
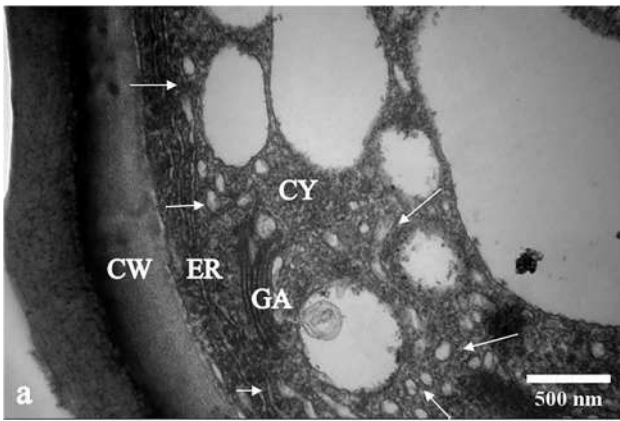


Fig. 5 Vacuole ultrastructural changes during stages of development and senescence of petal mesophyll cells of *Antirrhinum majus* “Legend White.” **a** Early stages of vacuolation (macroautophagy) at S1; **b** lateral fuse of tubular structures in the vacuolation process at S2; **c** spiral structure of the cytoplasm within the vacuole (microautophagy) at S2; **d** fusion of the vacuoles at S3; **e** central vacuole at S4 and **f** S5; **g** tonoplast rupture at S6; **h** central vacuole destruction at S7. CV central vacuole, CW cell wall, CY cytoplasm, ER endoplasmic reticulum, GA Golgi apparatus, M mitochondria, N nucleus, SV small vacuole

spherical, tubular, and crescent (Fig. 10e). Some vesicles differed significantly in diameter and electron density at S6 (Fig. 10f). At S7, various paramural bodies were often adjacent to the cell wall (Fig. 10g). At the final stage (S8), the vesicles were mainly adjacent to the cell wall, which was the only remaining cell structure (Fig. 10h).

MLB

At S1, a multilamellar body (MLB) with lower electron density was attached to small mitochondria and entered the central vacuole (Fig. 11a). In another position, an MLB existed inside a small bi-membrane vesicle attached to a chloroplast. This structure seemed that join the central vacuole (Fig. 11b). Besides, an MLB was freely found in the vacuole and densely appeared like a pellet (Fig. 11c). At S3, MLB was observed inside the vacuole (Fig. 11d) and in contact with the cytoplasm (Fig. 11e). During flower opening, no trace of multilamellar bodies was found. At the late stages of senescence, the MLB was observed alongside the mitochondria (Fig. 11f).

Discussion

Cell arrangement

Changes in the cell arrangement depend on species. Intercellular spaces and looseness in the developmental stages of buds allow the expansion of petal cells. These spaces reduce when the cells reach their maximum expansion. Generally, cell organization breakdown was observed at the final stages of vacuolar (autolytic) cell death, which was associated with cell collapse and cell wall fragmentation (O’Donoghue 2006). PCD leads to abnormalities in the cellular shape observed in carnation (Smith et al. 1992), *Hemerocallis* (Panavas and Rubinstein 1998), *Iris* (Van Doorn et al. 2003), and *Sandersonia* (O’Donoghue 2006).

Cell wall

In some processes, such as petal senescence, the cell wall can be partly or primarily degraded (Van Doorn et al. 2011;

Wertman et al. 2012). In *Dendrobium* (Kamdee et al. 2015), carnation, and *Hemerocallis* (O’Donoghue 2006), inflation, distortion, and eventual disappearance of the cell wall were observed in senescent flowers. Our results indicated a slight decrease in cell wall thickness during the bud development stages due to the flexibility and changes of the cell wall against the turgor pressure due to the increase in vacuole volume during petal development and flower opening (O’Donoghue 2006). During vacuolar cell death and before the degradation of the cell wall, the cell wall swells, and then its thickness decreases. In our results and Kamdee et al. (2015) studies, cell wall thickness measurements showed this event. It is generally believed that cell wall degradation is associated with turgor loss and cell collapse, paramural bodies containing degrading enzymes (Kamdee et al. 2015), tonoplast rupture, and the release of hydrolytic enzymes (Shibuya et al. 2016).

Plasma membrane

Our results indicate plasma membrane detachment from the cell wall and protoplast shrinkage occurred before tonoplast rupture. After that, the plasma membrane collapsed in parts. Early plasma membrane rupture and then protoplast shrinkage are features that differentiate plant PCD from necrosis. In protoplast shrinkage, the plasma membrane detaches from the cell wall (Van Doorn et al. 2011; Mondal et al. 2021), which is often irreversible and has been observed in stress-induced plant cell death (Minina et al. 2021). At S5, we observed protoplast shrinkage without plasma membrane rupture that has been reported during victorin-induced cell death. Plasma membrane rupture occurs most often after tonoplast rupture and the release of hydrolytic enzymes from the vacuoles (Van Doorn 2011; Van Doorn et al. 2011). We found the same results in our experiment.

Nucleus

The results indicated the nucleus remained until the beginning of petal wilting (S6) and completely disappeared at the last two stages. The nucleus morphology was different during development and cell death. During development, the nucleus had normal morphology, but from S3, an irregularity was observed in the nucleus structure, which could be due to the early onset of chromatin condensation. Chromatin condensation is a critical feature of apoptosis and the most obvious morphological change of the nucleus during vacuolar cell death that first occurs at the margins of the nucleus and then gradually throughout the nucleus and may happen before tonoplast rupture and complete clearance of the cytoplasm (Van Doorn et al. 2011; Van Doorn 2012). TEM micrographs in our results confirmed this event. Partial chromatin

Fig. 6 Mitochondria ultrastructural changes during stages of development and senescence of petal mesophyll cells of *Antirrhinum majus* “Legend White.” **a** Mitochondria natural ultrastructure at S1; **b** membrane structures of mitochondria at S2; **c** the elongated shape of mitochondria at S4 and **d** S5; **e** onset of crista degradation at S7; **f** significant reduction in mitochondria size at S8. C crista, M mitochondria

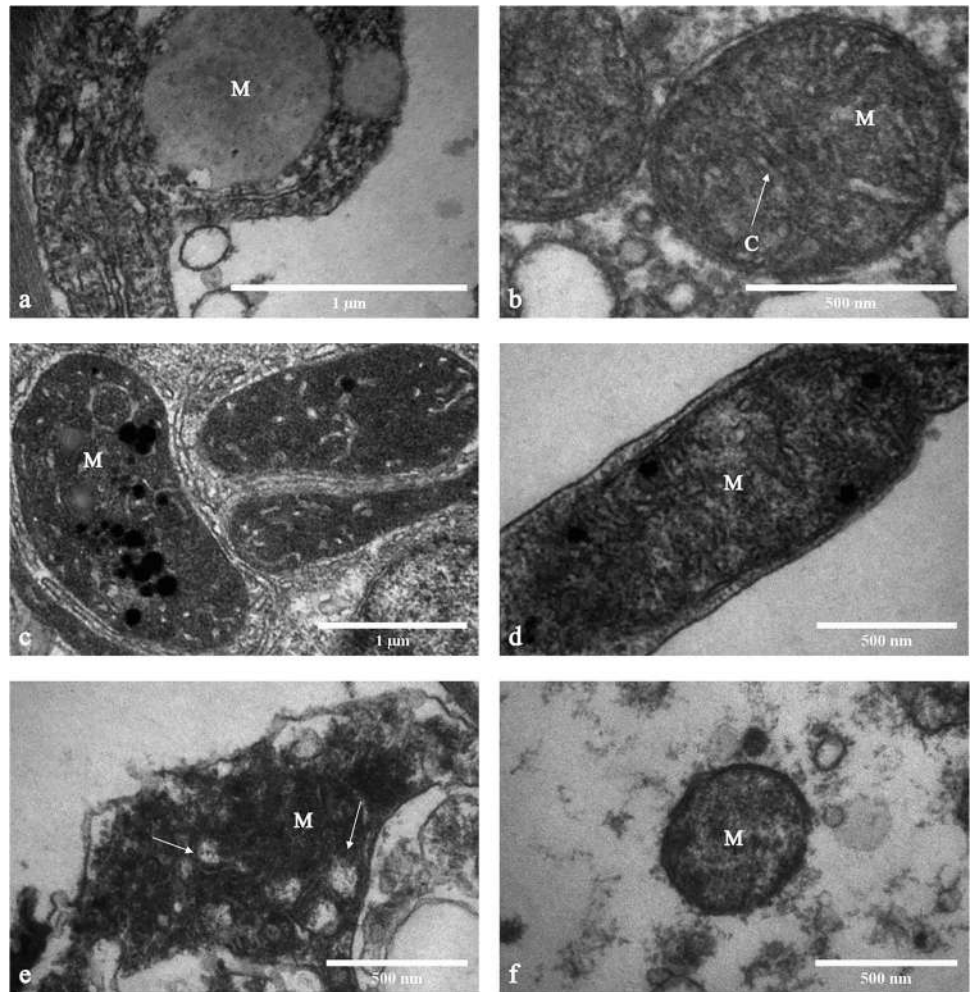


Fig. 7 Golgi apparatus ultrastructural changes during stages of development and senescence of petal mesophyll cells of *Antirrhinum majus* “Legend White.” **a** Golgi structure at S1 and **b** S2; **c** S3; **d** autophagosome-like structure of Golgi with cytoplasmic contents at S4. C cisternae, CF cis face, TF trans face

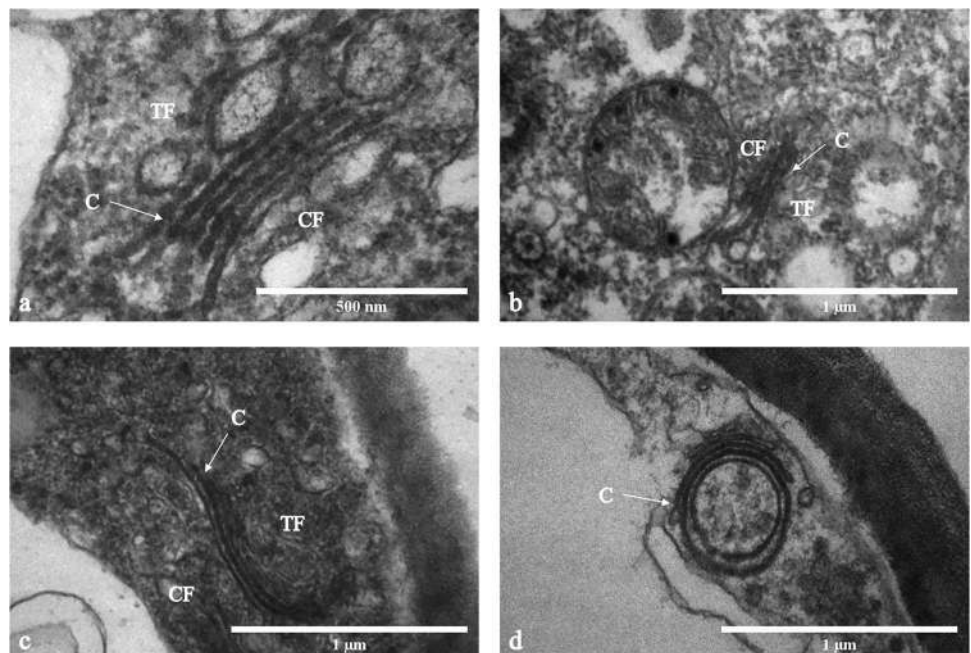


Fig. 8 Endoplasmic reticulum ultrastructural changes during stages of development and senescence of petal mesophyll cells of *Antirrhinum majus* “Legend White.” **a** Endoplasmic reticulum structure at S1 and **b** S5. CW cell wall, CY cytoplasm, ER endoplasmic reticulum

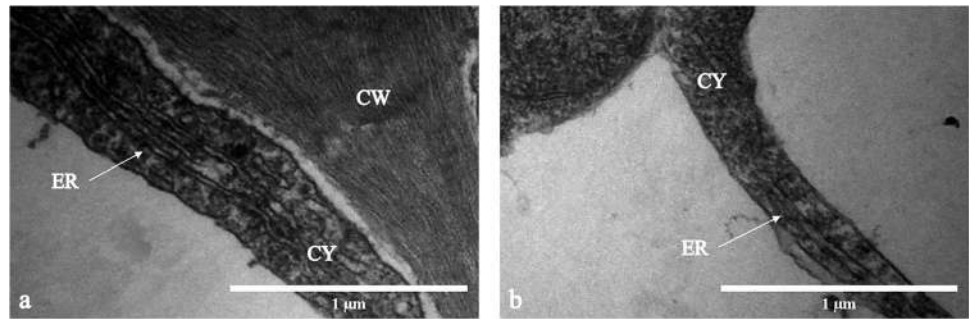
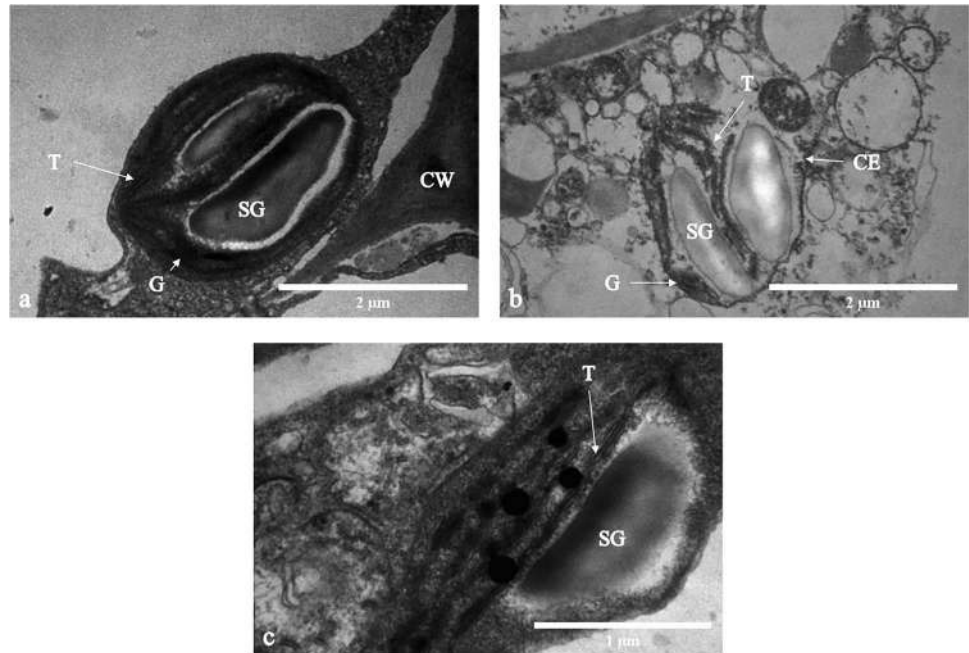
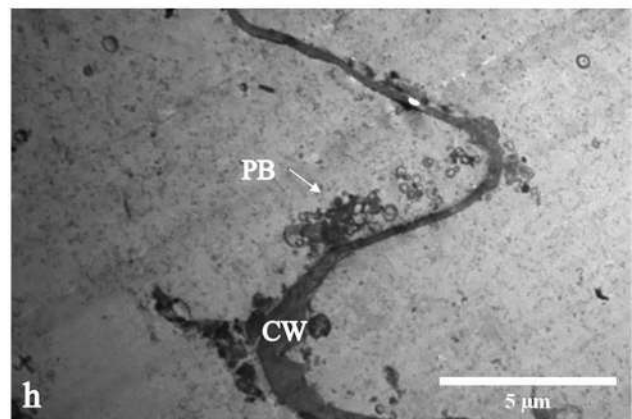
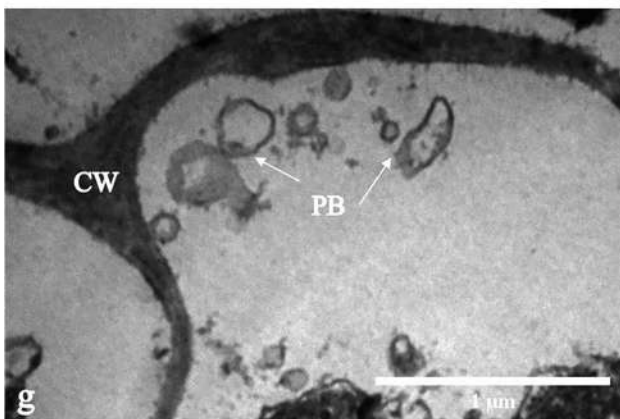
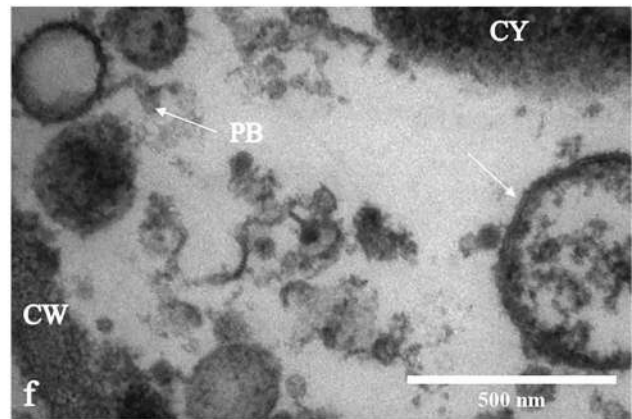
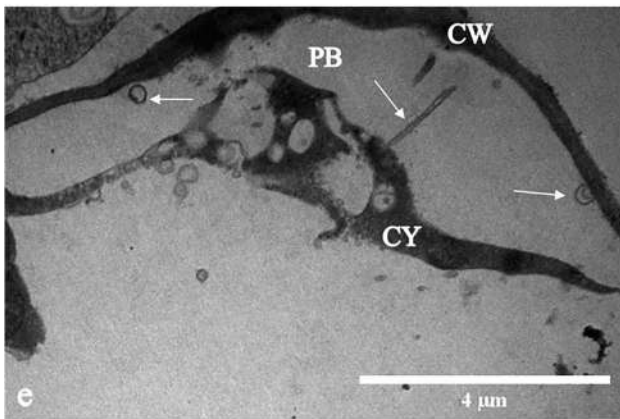
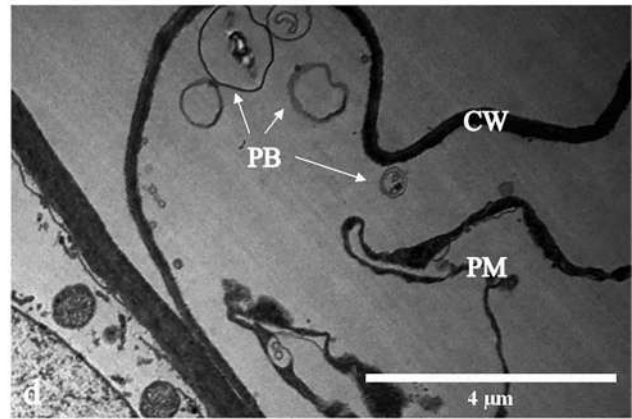
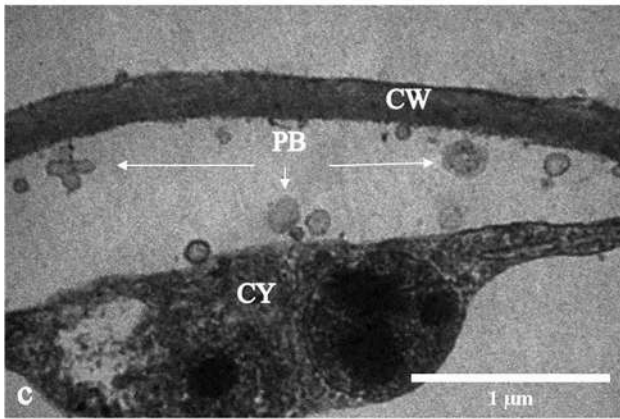
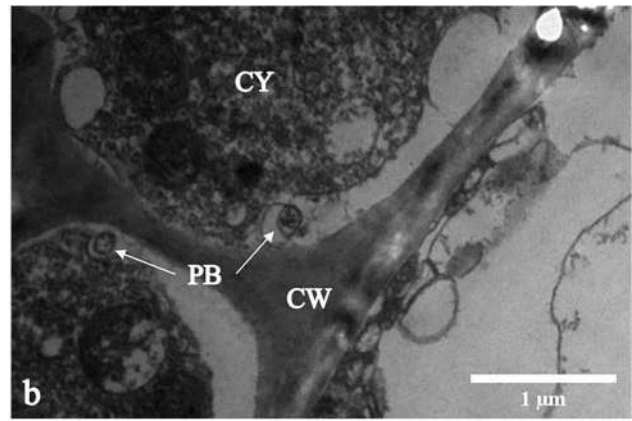
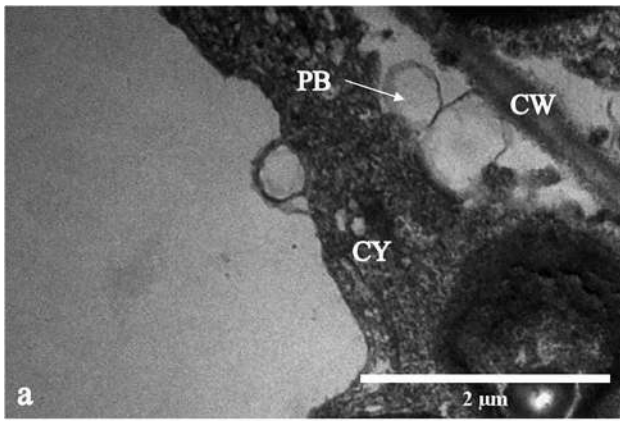


Fig. 9 Chloroplast ultrastructural changes during stages of development and senescence of petal mesophyll cells of *Antirrhinum majus* “Legend White.” **a** Normal chloroplast structure at S1; **b** chloroplast degradation at S2 and **c** S3. CE chloroplast envelope, CW cell wall, G grana, SG starch granule, T thylakoid



condensation from the full bud stage began progressively at the margin of the nucleus and was visible at the S5. At S5, a type of selective microautophagy was observed as known piecemeal microautophagy of the nucleus (PMN). PMN has been considered a specific feature of *Saccharomyces cerevisiae* and has not been found in other organisms (Sieńko et al. 2020). PMN occurs at nucleus-vacuole (NV) junctions where nonessential portions of the nucleus form teardrop-like blebs and protrude into the vacuole lumen (Roberts et al. 2003; Krick et al. 2008). PMN in *Saccharomyces cerevisiae* causes the degradation of nucleolus proteins and may play a role in nuclear degradation during vacuolar (autolytic) cell death (Sieńko et al. 2020). However, more studies are needed in this area. When the wilting began (S6), nucleus fragments were evident in most mesophyll cells. Furthermore, more electron density appeared on the nucleus surface, indicating chromatin condensation all over the nucleus, reducing

nucleus size. This event has been reported during vacuolar cell death of *Petunia*, *Argyranthemum*, *Antirrhinum* (Yamada et al. 2006), *Freesia*, *Gladiolus* (Shibuya et al. 2016), and *Ipomoea* (Van Doorn 2012). In another position, the nucleus was attached to a small vacuole at its smallest size, and a lower electron density was in the binding region. It appears that chromatin was accumulating on the side of the nucleus. After that, at S7 and S8, the nucleus completely disappeared. In animal systems, nucleus lack occurs with nuclear fragmentation, but this has rarely happened in plants. However, it has been reported in *Petunia* and *Argyranthemum* (Yamada et al. 2006) and our result, but not in *Antirrhinum* (Shibuya et al. 2016). In general, the complete collapse of the nucleus is attributed to tonoplast rupture (Yamada et al. 2006). The nuclear fragmentation may have occurred at intervals other than the sampling stages. However, its mechanism is still unknown.



◀**Fig. 10** Paramural bodies during stages of development and senescence of petal mesophyll cells of *Antirrhinum majus* “Legend White.” **a** Two vesicles with the membrane at S1 and **b** S2; **c** paramural bodies with or without membrane at S3; **d** vesicle containing smaller vesicle at S4; **e** vesicle with different shapes at S5; **f** vesicles with different diameter and electron density at S6; **g** paramural bodies adjacent to the cell wall at S7; **h** contact with the cell wall at S8. CW cell wall, CY cytoplasm, PB paramural body, PM plasma membrane

Vacuole

Ultrastructural changes in the vacuole were examined from two aspects. During development, the vacuolation (macroautophagy and microautophagy) occurred. During senescence and cell death, the vacuole played a central role (mega-autophagy) in vacuolar cell death. The vacuolation by cytoplasm expense is a form of autophagy (Van Doorn et al. 2015). Macroautophagy, microautophagy, and autophagy-like structures have been observed in *Ipomoea* (Phillips and Kende 1980), carnation (Smith et al. 1992), *Iris* (Van Doorn et al. 2003), *Dendrobium* (Van Doorn et al. 2015), and yeast. However, there is little evidence of autophagy processes in plants. During vacuolation, macroautophagy encloses part of the cytoplasm by an endoplasmic reticulum-derived membrane (Papini 2018). In our results, at S1 and S2, structures were formed in the cytoplasm that appeared to be different phases of macroautophagy if confined to a membrane. However, such a membrane was not observed, which does not mean it did not exist. In microautophagy, the cytoplasm is directly absorbed by tonoplast deformation, which eventually produces a vesicle released and degenerated inside the vacuole. Evidence of microautophagy is less than macroautophagy, but studies have suggested a hypothesis that microautophagy may be involved in vacuolation. At S2, TEM micrographs showed a process similar to microautophagy at high magnification. The initial phase of microautophagy, i.e., protrusion of the vacuolar membrane in the *Dendrobium*, has been shown (Van Doorn and Papini 2013; Van Doorn et al. 2015; Sienko et al. 2020). However, our results have a more advanced stage: entering part of the cytoplasm as a vesicle into the vacuole. It even seems that the membrane is formed. During development, several small vacuoles fused, increasing the volume of the vacuole, and eventually, the central vacuole occupied the entire cell at S4 and S5. There is another type of autophagy that is specific to plant cells. Mega-autophagy occurs at the final stage of vacuolar cell death and begins with tonoplast rupture (Van Doorn and Papini 2013). At S6, our results showed the tonoplast had ruptured some sections. No information is available on the processes that cause tonoplast rupture (Van Doorn 2012). In carnation, tonoplast rupture is followed by rapid clearance of the cytoplasm due to releasing large amounts of hydrolase from the vacuole. Autophagy-like structures may form in the cytoplasm before the tonoplast ruptures, apparently

responsible for the primary destruction of the cytoplasm (Van Doorn et al. 2011; Van Doorn 2012) that were observed at S6. Tonoplast rupture and vesicles destroyed the cytoplasmic content at the later stages.

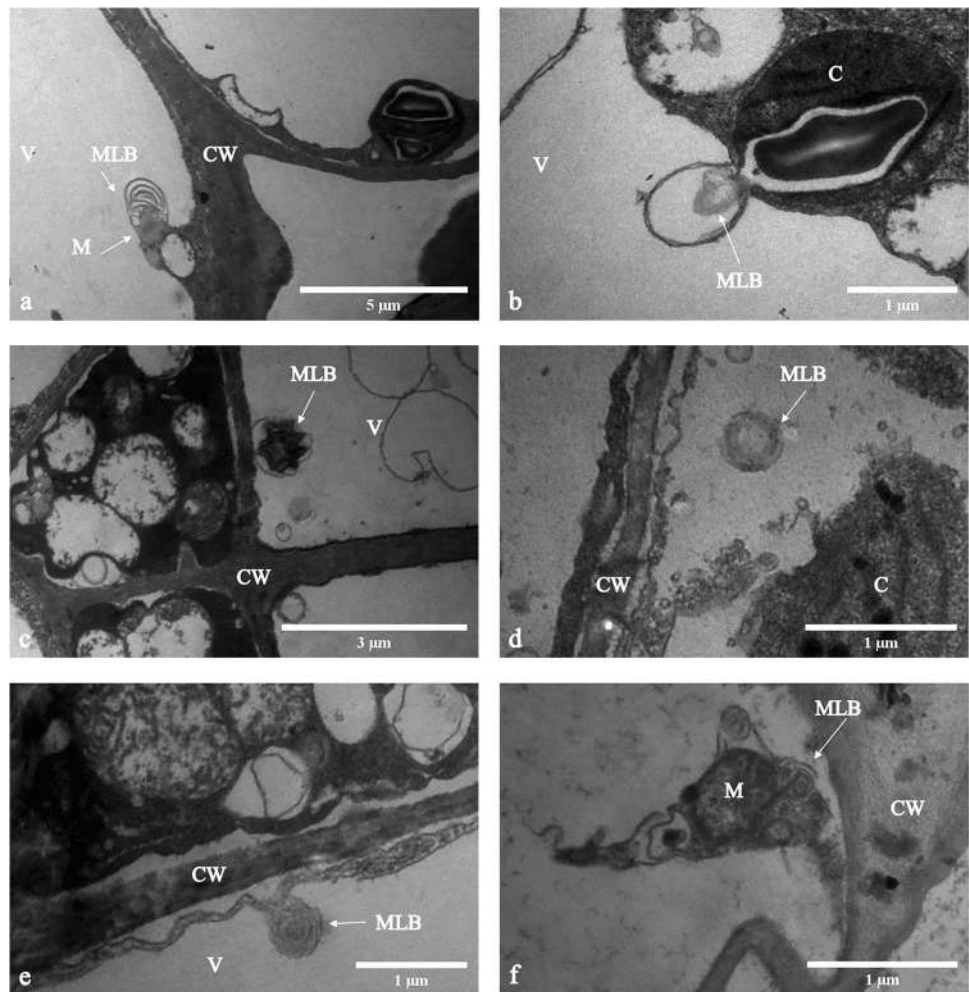
Mitochondria

Mitochondria are organelles that suffer minor structural damage during cell death (Adamakis and Eleftheriou 2019). During the development, there were many crista-rich mitochondria. At S4, the mitochondria were plentiful and elongated and had many electron dense granules on mitochondria's interior and peripheral surfaces. Mitochondrial elongation can occur for several reasons: this can lead to resistance to autophagic degradation or a solution to save energy (Vasileiou et al. 2019). Dense electron granules have been considered an indicator of mitochondrial development at later stages. In our results, such granules were the most numerous at the S4 and later stages. However, their number decreased and later wholly disappeared, such as in *Dendrobium* (Kirasak et al. 2010). When the cells were about to die, a slight degeneration was observed in the crista. Mitochondria were observed at the last stage of cell death, but their physiological status was unclear, as reported in carnation (Smith et al. 1992). Mitochondrial degradation occurs in animal systems through macroautophagy which has been shown in yeasts and root meristem cells (Adamakis and Eleftheriou 2019); however, no evidence of that has been found in other plant studies and our results.

Golgi apparatus

Golgi apparatus suffer the most severe structural damage during vacuolar (autolytic) cell death (Van Doorn 2011). Smith et al. (1992) showed the number of Golgi apparatus gradually decreases with the senescence of carnation cells. Our results also revealed that the number of Golgi apparatus gradually decreased during development. At S4, the Golgi apparatus was disrupted entirely, formed autophagosome-like structures, and disappeared after flower opening. It is not yet clear how the Golgi apparatus is degraded in plants. Golgi apparatus is fragmented in animals when exposed to various stresses (Hicks and Machamer 2005). In the study of autophagic pathways in the budding yeast *Saccharomyces cerevisiae*, there was a degradation pathway associated with the Golgi apparatus membrane. It was found significant changes occurred along this pathway in the Golgi apparatus. These changes included the elongation of the cisternae of the Golgi apparatus and their curvature, which eventually formed spherical bodies containing cytoplasmic components and organelles.

Fig. 11 Multilamellar bodies during stages of development and senescence of petal mesophyll cells of *Antirrhinum majus* “Legend White.” **a** A multilamellar body attached to the mitochondria and protruded into the central vacuole at S1; **b** an MLB inside a small bi-membrane vesicle and attached to a chloroplast at S1; **c** the presence of dense MLB in cell vacuoles at S1; **d** MLB near chloroplast in vacuole at S3; **e** MLB in contact with the cell cytoplasm at S3; **f** MLB alongside the remains of processing organelles at S8. C chloroplast, CW cell wall, M mitochondria, MLB multilamellar body, V vacuole



These structures were double-membrane chambers that acted like autophagosomes (Yamaguchi et al. 2016). In our results, similar changes occurred in the morphology of the Golgi apparatus, and structures were formed with two membranes, vesicles, and cytoplasmic contents. This event could be a possibility for autophagic activity in these structures.

Endoplasmic reticulum

The endoplasmic reticulum is a sensitive system during senescence and cell death and can be considered the initiator of PCD (Smith et al. 1992; Schäfer and Eichmann 2012). In studies of *Iris* senescence, the gradual disappearance of the endoplasmic reticulum and ribosomes was considered one of the first signs of senescence (Van Doorn and Woltering 2008). This study showed that the endoplasmic reticulum suddenly disappeared during vacuolar (autolytic) cell death. How the structure of this organelle was degraded during PCD has not yet been determined.

Chloroplast

Our result indicated that chloroplasts were present from S1 to S3. At S4 and after, no traces of plastids were observed. Some reports confirm the existence of these structures at the late stages of senescence along with mitochondria (Smith et al. 1992; Van Doorn 2011; Van Doorn and Prisa 2014). At S1, chloroplasts had normal morphology. But at the S2 and S3, they were altered and degraded. So, the chloroplast envelope membrane and the starch granules were degraded, and the granum collapsed. In the *Iris*, the main degradation of chloroplasts involves the gradual loss of grana and thylakoids (Van Doorn and Prisa 2014), which is similar to our results. Our results also indicated that at the S3, several dense electron globules were formed. These originate from Plastoglobuli. Plastoglobuli contain lipids and proteins present in plastids and may be involved in the breakdown of thylakoids. Dense electron globules have been observed in the senescence of soybeans, broccoli, and *Iris* and are thought to be involved in the degradation of plastids at the final stages of cell death (Shibuya et al. 2016).

Table 2 Morphological events during development and senescence of *Antirrhinum majus* “Legend White”

Stage	Morphological events
Tight green bud (S1)	Macroautophagy during vacuolation
Emerging bud (S2)	Macroautophagy, microautophagy, and fusion during vacuolation The onset of chloroplast degradation
Full bud (S3)	The onset of chromatin condensation Decrease in nucleolus number Decrease in number of the Golgi apparatus Changes in mitochondria morphology
Half-opened flower (S4)	Cell wall swelling Formation of the central vacuole Conversion of Golgi apparatus into the autophagosome-like structure Formation of granules on mitochondria surface The disappearance of chloroplast
Fully opened flower (S5)	Decrease in cell wall thickness Detachment of Plasma membrane Protoplasmic shrinkage Piecemeal microautophagy of the nucleus (PMN) and nuclear fragmentation The disappearance of the Golgi apparatus
Flower starting to wilt (S6)	Decrease in nucleus size The disappearance of the nucleolus Tonoplast rupture The disappearance of the endoplasmic reticulum
Collapsed flower (S7)	Plasma membrane rupture The disappearance of the nucleus Degradation of cristae in mitochondria
Desiccated flower (S8)	The disappearance of plasma membrane The disappearance of mitochondria The disappearance of cytoplasm

PB

PBs are vesicles of various sizes, shapes, and electron densities between the plasma membrane and the cell wall (Kirasak et al. 2010). Their origin may be plasma membrane, cytoplasm, Golgi apparatus, and endoplasmic reticulum (Marchant and Robards 1968; Robards and Kidwai 1969). Our results showed that these vesicular structures were in different sizes and shapes at all stages of flower development, senescence, and cell death, as has been reported in *Iris* and *Dendrobium*. The function of PB remains unknown. However, they may be involved in the release of destroying products or transfer of enzymes to the cell wall, leading to cell wall degradation (Kamdee et al. 2015). In the last stages of PCD, they were in contact with the cell wall. So, their role is probably cell wall breakdown. However, further studies of the function of PB are needed.

MLBs

MLB are structures with several concentric membrane layers located inside one vesicle. They are located in the cytoplasm or vacuole and have a role in storing protein and lipids and secreting lipids. Their origin is not yet known in plants, but in animals, they are composed of Golgi and autophagy (Van Doorn and Papini 2016). Studies of senescence have

suggested that there is another autophagy pathway in plants. This vacuole-independent pathway contains plastids that led to MLB formation (Van Doorn and Papini 2016; Papini 2018). In our results, MLB were often observed near chloroplasts at the bud stages and may have originated from them. Also, these structures were near degenerating mitochondria at S8 that seem to originate from the remnants of the cytoplasm.

In our study, PCD-related events in mesophyll cells began from flower bud stages and continued irreversibly, which confirmed the results of previous studies (Van Doorn et al. 2011; Van Doorn 2012). Unlike leaves, petal senescence is an irreversible process and synonymous with PCD and never stops. This is because developmental signals, rather than environmental signals, strongly regulate petal senescence (Ma et al. 2018). The early onset of PCD-related events has raised this question: how can a petal look fine while all these processes occur inside the petal? According to previous studies, autolysis of mesophyll cells in most species occur earlier than in other cells (epidermal cells and cells around the phloem tissue). The reason is plasmodesmata closure (Winkenbach 1971; Van Doorn and Woltering 2008; Shibuya et al. 2016). Also, the visible sign of senescence (or wilting) appears on petals when epidermal cells die (Van Doorn and Woltering 2008). Therefore, the petals look fine until the epidermal cells die. In general, the expression

of senescence-associated genes (SAGs) and signaling are controlled by time, and a monitoring network determines when the cell should die. However, early reception of the senescence signal by mesophyll cells compared to other cells leads to a change from the non-senescence stage to the senescence stage (Van Doorn et al. 2003; Van Doorn and Woltering 2008).

Conclusion

The present study investigated morphological events of *Antirrhinum majus* “Legend White” petals, and a sequence of events was obtained during vacuolar (autolytic) cell death. Morphological events are summarized in Table 2. Results indicated that cytoplasm and cellular organelles undergo a regular sequence of PCD-induced changes and gradually disappear. Evidence suggests that the cell died with rupture of the tonoplast and plasma membrane. Most events begin before the flower opens, and in some cases, autophagy processes were involved.

Examination of autophagy processes in *Antirrhinum majus* “Legend White” revealed unexpected aspects of autophagy. The vacuolation process showed both macroautophagy and microautophagy. Golgi apparatus became autophagosome-like organelles during vacuolar (autolytic) cell death and had autophagy activity. Golgi apparatus degeneration provided a better understanding of how autophagosome-like organelles originated. Our findings showed the presence of piecemeal microautophagy of the nucleus (PMN), which was previously observed in just one type of yeast. This observation is the first report of PMN in plants. The existence of autophagy structures and their formation process provided an excellent insight and basis for molecular studies. It is now believed that autophagic processes play a significant role in the progression of senescence and cell death. Therefore, molecular mechanisms involved in autophagy processes can now be studied with more assurance.

Acknowledgements We thank to Dr. Asadollah Asadi and Dr. Arash Abdolmaleki for the assistance in TEM analysis.

Author contribution R N S: data analyzer. E CH: supervision. Y P H: supervision. A E: advising. All authors read and approved the manuscript.

Funding This study was funded by the University of Mohaghegh Ardabili.

Data availability All data supporting the findings of the present study are available in this paper.

Declarations

Competing Interests The authors declare no competing interests.

References

- Adamakis I-DS, Eleftheriou EP (2019) Structural evidence of programmed cell death induction by tungsten in root tip cells of *Pisum sativum*. *Plants* 8:62. <https://doi.org/10.3390/plants8030062>
- Avci U, Earl Petzold H, Ismail IO et al (2008) Cysteine proteases XCP1 and XCP2 aid micro-autolysis within the intact central vacuole during xylogenesis in *Arabidopsis* roots. *Plant J* 56:303–315. <https://doi.org/10.1111/j.1365-313X.2008.03592.x>
- Azad AK, Ishikawa T, Ishikawa T et al (2008) Intracellular Energy Depletion Triggers Programmed Cell Death during Petal Senescence in Tulip. *J Exp Bot* 59:2085–2095. <https://doi.org/10.1093/jxb/ern066>
- Breeze E, Wagstaff C, Harrison E et al (2004) Gene expression patterns to define stages of post-harvest senescence in *Alstroemeria* petals. *Plant Biotechnol J* 2:155–168. <https://doi.org/10.1111/j.1467-7652.2004.00059.x>
- Chanoca A, Kovinich N, Burkel B et al (2015) Anthocyanin vacuolar inclusions form by a microautophagy mechanism. *Plant Cell* 27:2545–2559. <https://doi.org/10.1105/tpc.15.00589>
- Gaffal KP, Friedrichs GJ, El-Gammal S (2007) Ultrastructural evidence for a dual function of the phloem and programmed cell death in the floral nectary of *Digitalis purpurea*. *Ann Bot* 99:593–607. <https://doi.org/10.1093/aob/mcm002>
- Goto-Yamada S, Oikawa K, Bizan J et al (2019) Sucrose starvation induces microautophagy in plant root cells. *Front Plant Sci* 10:1–16. <https://doi.org/10.3389/fpls.2019.01604>
- Hicks SW, Machamer CE (2005) Golgi structure in stress sensing and apoptosis. *Biochim Biophys Acta (BBA)-Mol Cell Res* 1744:406–414. <https://doi.org/10.1016/j.bbamcr.2005.03.002>
- Kamdee C, Kirasak K, Ketsa S, van Doorn WG (2015) Vesicles between plasma membrane and cell wall prior to visible senescence of Iris and *Dendrobium* flowers. *J Plant Physiol* 188. <https://doi.org/10.1016/j.jplph.2015.02.013>
- Kirasak K, Ketsa S, Imsabai W, van Doorn WG (2010) Do mitochondria in *Dendrobium* petal mesophyll cells form vacuole-like vesicles? *Protoplasma* 241:51–61. <https://doi.org/10.1007/s00709-010-0105-0>
- Krick R, Muehe Y, Prick T et al (2008) Piecemeal microautophagy of the nucleus requires the core macroautophagy genes. *Mol Biol Cell* 19:4492–4505. <https://doi.org/10.1091/mbc.E08-04-0363>
- Ma N, Ma C, Liu Y et al (2018) Petal senescence: a hormone view. *J Exp Bot* 69:719–732. <https://doi.org/10.1093/jxb/ery009>
- Marchant R, Robards AW (1968) Membrane systems associated with the plasmalemma of plant cells. *Ann Bot* 32:457–471. <https://doi.org/10.1093/oxfordjournals.aob.a084221>
- Minina EA, Dauphinee AN, Ballhaus F et al (2021) Apoptosis is not conserved in plants as revealed by critical examination of a model for plant apoptosis-like cell death. *BMC Biol* 19:1–17. <https://doi.org/10.1186/s12915-021-01018-z>
- Mondal R, Antony S, Roy S, Chattopadhyay SK (2021) Programmed Cell Death (PCD) in Plant: Molecular Mechanism, Regulation, and Cellular Dysfunction in Response to Development and Stress. In: *Regulation and Dysfunction of Apoptosis*. IntechOpen, London, UK., pp 1–19. <https://doi.org/10.5772/intechopen.97940>
- Muhlemann JK, Maeda H, Chang C-Y et al (2012) Developmental changes in the metabolic network of snapdragon flowers. *PLoS ONE* 7:e40381. <https://doi.org/10.1371/journal.pone.0040381>
- Nakamura S, Hidema J, Sakamoto W et al (2018) Selective elimination of membrane-damaged chloroplasts via microautophagy. *Plant Physiol* 177:1007–1026. <https://doi.org/10.1104/pp.18.00444>

- O'Donoghue EM, Somerfield SD, Heyes JA (2002) Organization of cell walls in *Sandersonia aurantiaca* floral tissue. *J Exp Bot* 53:513–523. <https://doi.org/10.1093/jexbot/53.368.513>
- Odonoghue EM (2006) Flower petal cell walls: changes associated with flower opening and senescence. *New Zeal J For Sci* 36:130
- Panavas T, Rubinstein B (1998) Oxidative events during programmed cell death of daylily (*Heimerocallis* hybrid) petals. *Plant Sci* 133:125–138. [https://doi.org/10.1016/S0168-9452\(98\)00034-x](https://doi.org/10.1016/S0168-9452(98)00034-x)
- Papini A (2018) Investigation of morphological features of autophagy during plant programmed cell death. *Methods Mol Biol* (clifton, NJ) 1743:9–19. https://doi.org/10.1007/978-1-4939-7668-3_2
- Papini A, Mosti S, Brighigna L (1999) Programmed-cell-death events during tapetum development of angiosperms. *Protoplasma* 207:213–221. <https://doi.org/10.1007/BF01283002>
- Phillips HL, Kende H (1980) Structural changes in flowers of *Ipomoea tricolor* during flower opening and closing. *Protoplasma* 102:199–215. <https://doi.org/10.1007/BF01279588>
- Rabiza-Świder J, Skutnik E, Jędrzejuk A, Rochala-Wojciechowska J (2020) Nanosilver and sucrose delay the senescence of cut snapdragon flowers. *Postharvest Biol Technol* 165:111165. <https://doi.org/10.1016/j.postharvbio.2020.111165>
- Reynolds ES (1963) The use of lead citrate at high pH as an electron-opaque stain in electron microscopy. *J Cell Biol* 17:208. <https://doi.org/10.1083/jcb.17.1.208>
- Robards AW, Kidwai P (1969) Vesicular involvement in differentiating plant vascular cells. *New Phytol* 68:343–349. <https://doi.org/10.1111/J.1469-8137.1969.TB06446.X>
- Roberts P, Moshitch-Moshkovitz S, Kvam E et al (2003) Piecemeal microautophagy of nucleus in *Saccharomyces cerevisiae*. *Mol Biol Cell* 14:129–141. <https://doi.org/10.1091/mbc.e02-08-0483>
- Rogers HJ (2015) Senescence-associated programmed cell death. In: *plant programmed cell death*. Springer International publishing, Switzerland, pp 203–233. https://doi.org/10.1007/978-3-319-21033-9_9
- Schäfer P, Eichmann R (2012) The endoplasmic reticulum in plant immunity and cell death. *Front Plant Sci* 3:200. <https://doi.org/10.3389/fpls.2012.00200>
- Shibuya K, Yamada T, Ichimura K (2016) Morphological changes in senescing petal cells and the regulatory mechanism of petal senescence. *J Exp Bot* 67:5909–5918. <https://doi.org/10.1093/jxb/erw337>
- Sienko K, Poormassalehgoo A, Yamada K, Goto-Yamada S (2020) Microautophagy in plants: consideration of its molecular mechanism. *Cells* 9:887. <https://doi.org/10.3390/cells9040887>
- Smith MT, Saks Y, van Staden J (1992) Ultrastructural changes in the petals of senescing flowers of *Dianthus caryophyllus* L. *Ann Bot* 69:277–285. <https://doi.org/10.1093/oxfordjournals.aob.a088341>
- Van Doorn WG (2011) Classes of programmed cell death in plants, compared to those in animals. *J Exp Bot* 62:4749–4761. <https://doi.org/10.1093/jxb/err196>
- Van Doorn WG, Papini A (2013) Ultrastructure of autophagy in plant cells: a review. *Autophagy* 9:1922–1936. <https://doi.org/10.4161/auto.26275>
- Van Doorn WG, Papini A (2016) Plastid degeneration in *Tillandsia albida* (Bromeliaceae) and *Lobivia rauschii* (Cactaceae) provides evidence about the origin and destiny of multilamellar bodies in plants. *Phytomorphology* 66:103–112. <https://doi.org/10.1101/038158>
- Van Doorn WG, Prisa D (2014) Lipid globules on the plastid surface in *Iris* tepal epidermis cells during tepal maturation and senescence. *J Plant Physiol* 171:1714–1721. <https://doi.org/10.1016/j.jplph.2014.08.003>
- Van Doorn WG, Woltering EJ (2008) Physiology and molecular biology of petal senescence. *J Exp Bot* 59:453–480. <https://doi.org/10.1093/jxb/erm356>
- Van Doorn WG, Balk PA, Van Houwelingen AM et al (2003) Gene expression during anthesis and senescence in *Iris* flowers. *Plant Mol Biol* 53:845–863. <https://doi.org/10.1023/B:PLAN.0000023670.61059.1d>
- Van Doorn WG, Beers EP, Dangl JL et al (2011) Morphological classification of plant cell deaths. *Cell Death Differ* 18:1241–1246. <https://doi.org/10.1038/cdd.2011.36>
- Van Doorn WG (2012) Programmed cell death in cut flowers. In: *Proceedings of the Xth international symposium on postharvest quality of ornamental plants*. Pernambuco, Brazil, pp 35–38
- Van Doorn WG (2015) Programmed cell death in cut flowers. *Acta Hort* 1060:35–38. <https://doi.org/10.17660/ActaHortic.2015.1060.4>
- Van Doorn WG, Kirasak K, Ketsa S (2015) Macroautophagy and microautophagy in relation to vacuole formation in mesophyll cells of *Dendrobium* tepals. *J Plant Physiol* 177:67–73. <https://doi.org/10.1016/j.jplph.2015.01.006>
- Vasileiou PVS, Evangelou K, Vlasik K et al (2019) Mitochondrial Homeostasis and Cellular Senescence. *Cells* 8:686. <https://doi.org/10.3390/cells8070686>
- Wagstaff C, Malcolm P, Rafiq A et al (2003) Programmed cell death (PCD) processes begin extremely early in *Alstroemeria* petal senescence. *New Phytol* 160:49–59. <https://doi.org/10.1046/j.1469-8137.2003.00853.x>
- Wertman J, Lord CEN, Dauphinee AN, Gunawardena AH (2012) The pathway of cell dismantling during programmed cell death in lace plant (*Aponogeton madagascariensis*) leaves. *BMC Plant Biol* 12:1–17. <https://doi.org/10.1186/1471-2229-12-115>
- Winkenbach F (1971) Function of lysosomes and lysosomal enzymes in the senescing corolla of the morning glory (*Ipomoea purpurea*). *J Exp Bot* 23:759–771. <https://doi.org/10.1093/jxb/22.4.759>
- Yamada T, Ichimura K, van Doorn WG (2006) DNA degradation and nuclear degeneration during programmed cell death in petals of *Antirrhinum*, *Argyranthemum*, and *Petunia*. *J Exp Bot* 57:3543–3552. <https://doi.org/10.1093/jxb/erl100>
- Yamaguchi H, Arakawa S, Kanaseki T et al (2016) Golgi membrane-associated degradation pathway in yeast and mammals. *EMBO J* 35:1991–2007. <https://doi.org/10.15252/embj.201593191>
- Zhao L, Xia Y, Wu XY et al (2018) Phenotypic analysis and molecular markers of leaf senescence. *Methods Mol Biol* 1744:35–48. https://doi.org/10.1007/978-1-4939-7672-0_3

Publisher's note Springer Nature remains neutral with regard to jurisdictional claims in published maps and institutional affiliations.